JP Journal of Heat and Mass Transfer

Published Online: May 2014
Available online at http://pphmj.com/journals/jphmt.htm
Volume 9, Number 1, 2014, Pages 1-19

HEAT AND MASS TRANSFER ANALYSIS IN A ROTARY WHEEL

Koutama Amara, Ridha Chouikh and AmenAllah Guizani

LMTE/CRTEn BP 95 Hammam Lif 2050, Tunisia
e-mail: koutamaradhia@yahoo.fr
ridha.chouikh@ipein.rnu.tn
amenallah.guizani@crten.rnrt.tn

Abstract

This article presents a study of energy recovery ventilator in the form of sensible and latent (wheel condensation with porous walls). A mathematical model is governing the equations describing the heat and mass transfer, counter-current air circulations. This has been numerically solved for the condensation model. By using this method, the finite volume has been solved using the partial differential equations (PDE). The numerical model has been developed to study and discuss the parameters' effect such as the thickness of the wheel, the rotational speed, porosity and air flow rate on the effectiveness of the wheel. The results show that the effectiveness changes exponentially until reaching a cyclic equilibrium after about 50 cycles. Moreover, the effectiveness decreases with increasing flow rate. These results are in agreement with those reported in the literature.

Nomenclature

A_s : Convective heat and mass transfer surface area $[\mathrm{m}^2]$

Cp_g : Specific heat of the gas $[\mathrm{J/kg^{\circ}K}]$

Received: October 12, 2013; Revised: December 18, 2013; Accepted: February 1, 2014
Keywords and phrases: recovery energy, heat and mass transfer, condensation wheel, effectiveness sensible, effectiveness latent, effectiveness total.

Cp_m : Specific heat of the matrix $[\mathrm{J/kg^{\circ}K}]$

Cp_{wl} : Specific heat of water vapour $[\mathrm{J/kg^{\circ}K}]$

C_r : Capacity-ratio of the rotary (matrix) $[\mathrm{W/S}]$, $C_r = (MCp)_m \Omega$

C_g : Gas capacity rates $[\mathrm{W/S}]$, $C_g = (mCp)_g$

C_r^+ : Heat capacity-rate of the rotary wheel $C_r^+ = \dfrac{C_r}{C_g}$

D : Diameter of the wheel $[\mathrm{m}]$

Fo_m : The Fourier number of matrix

h_{vap} : Specific heat of vaporization $[\mathrm{KJ/kg}]$

h_{HT} : Convective heat transfer coefficient $[\mathrm{W/m^{2\circ}k}]$

h_{MT} : Mass transfer coefficient $[\mathrm{kg/ms}]$

K_m : Thermal conductivity of the matrix $[\mathrm{W/m^{\circ}k}]$

L : Length of regenerator $[\mathrm{m}]$

m_g : Mass flow rate gas $[\mathrm{kg_{da}/s}]$

Nu : Nusselt number

P_a : Atmospheric pressure $[\mathrm{P_a}]$

Q : Volume flow rate $[\mathrm{m^3/s}]$

Re : Reynolds number

NTU_{HT} : Number of the heat transfer unit

NTU_{MT} : Number of the mass transfer unit

T_g : Temperature of the gas (air stream) $[\mathrm{K}]$

T_g^+ : Non-dimensional temperature of gas

T_m : Temperature of matrix [K]

T_m^+ : Non-dimensional temperature of matrix

t : Time [s]

$t^+ = \frac{t}{\tau}$: Non-dimensional time

x : Axial coordinate [m]

$x^+ = \frac{x}{L}$: Non-dimensional length

U_g : Superficial mean gas velocity [m/s]

ΔT_g : Temperature difference between supply and exhaust inlet conditions [K]

$\Delta\omega_g$: Humidity ratio difference between supply and exhaust inlet conditions $[kg_{wv}/kg_{da}]$

ω_g^+ : Humidity ratio of moister air (water content in dry air) $[kg_{wv}/kg_{da}]$

ω_s^+ : Humidity ratio in equilibrium with matrix surface (saturated) $[kg_{wv}/kg_{da}]$

ω_m^+ : Humidity ratio of moister matrix

ϖ_m^+ : Moisture content of matrix $[kg_{wv}/kg_{dm}]$

ϖ_{max} : Loading of desiccant at 100% relative humidity, $[kg_{wv}/kg_{dm}]$

ρ_g : Density of the gas $[kg/m^3]$

ρ_{da} : Density of the dry air $[kg/m^3]$

ρ_m : Density of matrix $[kg/m^3]$

ϕ : Humidity ratio $[kg_{wv}/kg_{dm}]$

ε_s : Sensible energy wheel effectiveness

ε_l : Latent energy wheel effectiveness

ε_{tot} : Total energy wheel effectiveness

φ : Porosity of the matrix

Ω : Rotational speed [rpm]

Γ : Dimensionless period

Subscripts

a : air

c : cold flow stream

d : desiccant

da : dry air

e : exhaust flow to the energy wheel

g : gas flow

h : hot flow stream

i : inside flow to the wheel or at a point "*I*" in *x*-space direction

j : at point *j* in *y*-space direction of the regenerator

l : water liquid

m : matrix surface

min : minimum value

max : maximum value

o : outside flow from the wheel

s : supply flow to the energy wheel

1. Introduction

The amount of the work accomplished in the energy recovery field has increased in the last years. There is a growing demand for a better understanding of the transport phenomena and the phase change kinematics to optimize the cycles of the process. However, the majority of the works are numerical studies and there are few experimental attempts regarding the realistic total energy wheel.

One of the early experimental studies has been realized by Van Leersum and Ambrose [1]. He has dealt with a wheel with uncoated flow passages which precludes moisture transfer. More recently, experiments which coated flow passages were reported by Simpson et al. [2] for a unique configuration in which only a quarter of the face area of the rotating disk was exposed to each of the air streams. Thereafter, an experimental investigation has been carried out by Sparrow [3] in order to determine the operation performance of a rotating regenerative total energy wheel. The attributes of high accuracy, convenient operation low cost and flexibility with regard to the accommodation to many type of heat/moisture exchanger are the hallmarks of the presented test facility. Mandegari and Pahlavanzadeh [4] presented an experimental study relative to the operation of the desiccant wheel in the different climates and operating conditions. They have found that in different climates, all the described efficiencies decrease by the inlet temperature except the adiabatic efficiency which has an optimum point.

However, the literature contains a considerable number of numerical simulations because of the complexities of the experimental setup. One of the earlier studies is of Maclaine-Cross [5]. They have first discussed the problem of condensation forming inside a sensible heat regenerator. As

continuation of Maclaine-Gross's work, Van Leersum [6] has investigated the performance of a sensible wheel in which condensation occurs. Simonson and Besant [7] have derived the fundamental dimensionless groups of air-to-air energy wheels from the governing non-linear, coupled heat and moisture transfer equations. The dimensionless groups were used in Part II in order to develop effectiveness correlations for energy wheels. Moreover, Ahmed and Kattab [8] have described the honeycomb desiccant of rotary wheel which is constructed from iron wire and clothes layer and impregnated with calcium chloride solution. The honeycomb is used for regeneration and absorption processes. The results have shown that the wheel effectiveness of the solid desiccant is relatively higher than the one of the liquid desiccant at high flow rate.

In modelling heat and moisture transfer in non-desiccant and desiccant wheels, Kabeel [9] has introduced a wave analysis to establish a one-dimensional transient model of the rotary heat and mass exchanger.

Abdulmajeed and Al-Ghamdi [10] have introduced a wave analysis in order to establish a one-dimensional transient model of the rotary heat and mass exchanger. For modelling air-to-air wheel, three models have been developed: the sensible model, the condensation model, and the enthalpy model.

Nobrega and Brum [11] have developed a simple mathematical model to describe the heat and mass transfer in rotary exchangers. An effectiveness-number of thermal units (NTU) analysis has been carried out and the results have revealed that heat wheels can be far less efficient than enthalpy recovery wheels, depending on the atmospheric conditions.

These studies have shown the beneficial effects of discretization in partial equations as well as the configuration limitation. However, the condensation wheel model has not been the subject of theoretical study by finite volume techniques which are based on an integral-based method characterized by a high stability and a reduction in the total computational time. The elliptic matrix equations are approximated by using an explicit

finite volumes scheme while the elliptic governing equations of air stream are solved by using an integral-based scheme with explicit discretization in time coupled with an upwind method. Indeed, this model could mainly improve heat and mass transfer in whole configuration wheel condensation. Although, these studies have proven that the dehumidifier wheel is the main component of the solid desiccant system and that system effectiveness can be significantly improved by improving its performance, the existing works are not sufficiently detailed on the effect of the velocity and the operating parameters on wheel performance.

To date, the numerical study based on transfer heat and mass transfer related to the wheel symmetry and taking into consideration the parabolic equation has not been yet studied.

This work deals indeed with the mathematical models including the governing equations, the dimensionless representation, and the numerical approach. For the modelling of air-to-air rotary wheel, this model has been developed and used in order to examine the effectiveness of the wheel under summer and winter conditions. The model has been based on the physical principles of the operation of the energy wheels and they are considered to be one-dimensional and transient. Similarly, the governing equations with boundary and initial conditions have been derived to describe heat and mass transfer in air and the solid matrix.

2. Theoretical Model

Energy recovery technologies known as heat recovery ventilators or energy recovery ventilators use a rotary air-to-air energy wheel as a main part of its components. The air-to-air rotary energy wheel under investigation is a balanced counter flow and symmetric type. It is a rotating cylindrical wheel of length L and diameter D and it is divided into two equal sections: supply and exhaust. A typical operating condition would be warm humid supply air transferring energy and water vapor to the matrix and energy and moisture being transferred from the matrix to the exhaust air during the

second half of the cycle. The governing equations, presented in this section, have used the nomenclature and the coordinate system shown in Figure 1 which contains a scheme of an energy wheel operating in a counter flow arrangement. The supply side flow is denoted by subscript "*s*" and the exhaust side flow by "*e*". The subscripts "*I*" and "*o*" refer respectively to inflow and outflow. The axial coordinate "*x*" is defined as positive in the flow direction so that in the counter flow configuration, the axial coordinate reverses direction at the beginning of each side. Thereby, the coordinate "$x = L$" in the supply period becomes "$x = 0$" in the exhaust period.

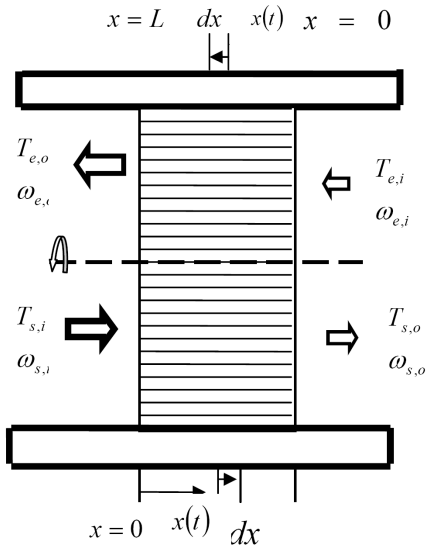

Figure 1. Nomenclature and coordinate system for the energy wheel.

This has enabled us to use the same differential equations for both hot and cold periods.

We have made several assumptions in order to help us in the model setup:

1. No mixing of the flow between the supply and exhaust section.
2. The effect of a small pressure drop on thermodynamic properties changes of air and the matrix is negligible.

3. The carry-over of air due to the wheel switching from one period to the other is neglected because the mass of this air is small compared to the mass of the matrix.
4. The radial gradients of temperature and moisture are neglected for both the matrix and the gas phases.
5. The axial heat conduction and axial mass diffusion in air are negligible.
6. The axial diffusion of moisture within the matrix is negligible.
7. The heat and mass transfer coefficients for both periods are considered to be identical and do not vary in time and space.
8. The air flow is one-dimensional.
9. The thermal and physical properties of the air and the silica gel do not change in the range of the operating temperature.
10. The system is considered adiabatic.
11. Each strip has a uniform temperature and moisture content.

Based on the above assumptions, the governing equations of the coupled heat and moisture transfer (condensation model) can be expressed as follows:

The condensation model:

The energy conservation equations are similar to that for the rotary sensible. However, there is an extra term added to the equation which indicates that energy is transferred in two different ways. As in the sensible case, there is an energy transfer due to the temperature gradient between the air stream and the matrix. Energy is also transferred with the water vapor. The energy stream is called *latent energy* and is due to the enthalpy.

The partial differential equations for describing the heat and mass transfer in the desiccant dehumidifier can be written as:

In the flow region:

Mass balance of water vapor in the gas phase:

$$\frac{1}{\Gamma}\frac{\partial \omega_g^+}{\partial t^+} + \frac{\partial \omega_g^+}{\partial x^+} + NTU_{MT}\ sign(\omega_g^+ - \omega_s^+)(\omega_g^+ - \omega_s^+) = 0. \quad (1)$$

Energy balance of the gas phase:

$$\frac{1}{\Gamma}\frac{\partial T_g^+}{\partial t^+} + \frac{\partial T_g^+}{\partial x^+} + NTU_{HT}(T_g^+ - T_m^+) = 0. \quad (2)$$

In the solid matrix:

Mass balance of liquid water on the matrix:

$$\frac{\partial \omega_m^+}{\partial t^+} = \frac{NTU_{MT}}{C_r^+}\frac{Cp_m}{Cp_g}\frac{\Delta\omega_g}{\varpi_{\max}} sign(\omega_g^+ - \omega_s^+)(\omega_g^s - \omega_s^+). \quad (3)$$

Energy balance of the matrix:

$$\frac{\partial T_m^+}{\partial t^+} - Fo_m\frac{\partial^2 T_m^+}{\partial x^{+2}} - \frac{NTU_{MT}}{C_r^+}(T_g^+ - T_m^+)$$

$$-\frac{NTU_{MT}}{C_r^+}\frac{h_{vap}\Delta\omega_g}{\Delta T_g Cp_g} sign(\omega_g^+ - \omega_s^+)(\omega_g^+ - \omega_s^+)$$

$$-\frac{NTU_{MT}}{C_r^+}\frac{Cp_{wl}}{Cp_g}\Delta\omega_g\ sign(\omega_g^+ - \omega_s^+)(\omega_g^+ - \omega_s^+)(T_g^+ - T_m^+) = 0. \quad (4)$$

In the above equation, C_r^+ is the heat capacity rate of the rotary wheel: $C_r^+ = \frac{C_r}{C_g}$. The capacity rate of the rotary (matrix) is defined: $C_r = (MCp)_m\Omega$ and the gas capacity rate is express as: $Cg = (mCp)_g$.

The initial and boundary conditions are:

$$T_g(x, 0) = T_{amb} = T_0; \quad T_m(x, 0) = T_{amb} = T_{m0},$$

$$T_g(0, t) = T_{in}; \quad \frac{\partial T_g(L, t)}{\partial x} = \frac{\partial T_m(L, t)}{\partial x} = 0,$$

where T_g^+ and T_m^+ are the dimensionless temperatures of gas and solid matrix, respectively, ω_g and ω_m are the humidity ratio and the water uptake, respectively.

Equations (1)-(4) form a set of transient one-dimensional coupled parabolic differential equations. This coupling is a result of two different effects. First, as described above, there is both a sensible and a latent term in the energy equations.

In the operation of regenerator (energy wheel), the regular periodic flow conditions are assumed to be achieved for design purpose. The solution to the governing differential equations is commonly presented in terms of the regenerator effectiveness as a function of the dimensionless parameters. ASHRAE [12] defines effectiveness as:

$$\varepsilon_{wheel} = \frac{Actual\ transfer(of\ \ moister\ or\ energy)}{Maximum\ possible\ transfer\ between\ air\ streams}.$$

This effectiveness can be written as follows:

$$\varepsilon_{wheel} = \frac{m_{supply}(\overline{Y}_{s,i} - Y_{s,i})}{\min(\dot{m}_{supply}, \dot{m}_{exhaust})(Y_{e,i} - Y_{s,e})}$$

ε_{wheel} sensible ε_s, latent ε_L or total effectiveness ε_T

Y temperature T_g, humidity ratio w_g or enthalpy h_g

$Y_{i,j}$ $i = s, e,$ (s : supply gas and e: exhaust gas) and $j = i, o,$ (i : supply and exhaust side in-flow, o: supply and exhaust side out-flow)

$\overline{Y_{i,j}}$ the time averaged value

$$\overline{Y_{s,o}} = \frac{1}{\tau_1}\int_0^{\tau_1} Y_{s,o}dt$$

and

$$\overline{Y_{e,o}} = \frac{1}{\tau_2}\int_0^{\tau_2} Y_{e,o}dt.$$

3. Solution Procedure

The mathematical model of heat transfer in sensible wheel or heat and mass transfer in condensation wheel are coupled and partial differential equations with the given boundary and periodic equilibrium conditions. The numerical calculations by finite volume techniques are based on an integral-based method characterized by a high stability and a reduction in the total computational time. The parabolic matrix equations are approximated by using a full-implicit finite volume scheme while the parabolic governing equations of the air stream are solved by using an integral-based scheme with implicit discretization in time coupled with an upwind method. The obtained tri-diagonal systems of matrix equations are efficiently solved by means of Fortran algorithm. The same equations can be used for both the supply and the exhaust sides since the direction of the air flow goes with positive *x*-axis for the two air streams. The sequence of the code begins by the resolution at each time-step of the temperature and water content of both the air and the solid matrix along the length of the wheel (*x* direction) until the end of each period. Then, the results are recorded and stored for effectiveness and next period calculations. This process is repeated until the residuals agree with the specified values. It is to be noted here that the matrix surface condition (dry or wet) was checked at each grid point to study the possibility of evaporation to occur. The sequence of calculations is repeated for each cycle until cyclic equilibriums are reached. In the present study, and after series of running trials, the number of grid points in the *x*-direction is fixed at 300 while the number of time-step is fixed at 100 for all cases.

4. Numerical Results

This work is focused to analyse the two numerical models, presented above. The air-to-air rotary energy wheel under investigation is balanced and symmetric. The basic physical parameters and relation describing the rotary energy wheel are summarized in Table 1. The typical operating conditions in the winter (heating mode) and summer (cooling mode) are listed in Table 2.

Table 1. Wheel parameters and matrix properties used in numerical analysis

Air : Volume flow rates $\dot{Q}_{\text{sup}} = \dot{Q}_{exch} = 300[\text{CMH}]$				
Rotation speed of wheel $\Omega = 30[\text{rpm}]$				
$L = 0.04\,\text{m}$	$\varphi = 92.5\%$	$U_s = 1.1\,\text{m/s}$	$C_r^+ = 4.6$	$A_s = 4026\,\text{m}^2$
Matrix properties : Linear Isotherm				
$Cp_m = 1340\,[\text{J/Kg K}]$		$\rho_m = 1380\,[\text{Kg/m}^3]$	$K_m = 0.16\,[\text{w/m K}]$	

Table 2. (a) Boundary conditions used in numerical analysis (summer run) sensible wheel. (b) Boundary conditions used in numerical analysis (winter run) condensation wheel

(a)

Test mode	Supply air conditions		Exhaust air conditions	
	$T_g\,(^\circ\text{C})$	$\phi_g\,[\text{Kg}_{\text{wv}}/\text{Kg}_{\text{dm}}]$	$T_g\,(^\circ\text{C})$	$\phi_g\,[\text{Kg}_{\text{wv}}/\text{Kg}_{\text{dm}}]$
In side	35	0.0174	24	0.0092
Out side	24.5	0.011	34.5	0.0165

(b)

Test mode	Supply air conditions		Exhaust air conditions	
	$T_g\,(^\circ\text{C})$	$\phi_g\,[\text{Kg}_{\text{wv}}/\text{Kg}_{\text{dm}}]$	$T_g\,(^\circ\text{C})$	$\phi_g\,[\text{Kg}_{\text{wv}}/\text{Kg}_{\text{dm}}]$
In side	4	0.0038	22	0.0070
Out side	18	0.0056	7	0.0047

The dimensionless temperature distribution of the air stream and matrix for both supply and exhaust periods is shown at the steady state in Figures 2 and 3. The steady condition is reached when the difference in effectiveness of each cycle is within the specification. We remark that the temperature distribution in the hot gas flow period for the matrix is lower than the air stream which means the transfer is from the hot air to the matrix surface. In the case of the cold period, the scenario is opposite which leads the heat transfer to flow from the matrix surface of the cold air flow.

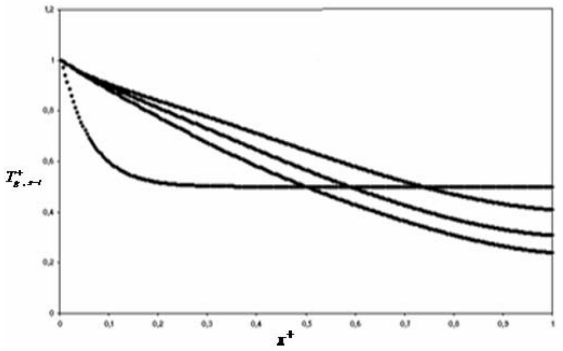

Figure 2. Dimensionless temperature distribution for the air during the hot period (summer). The set of data lines shows progression to the steady state from the initial point.

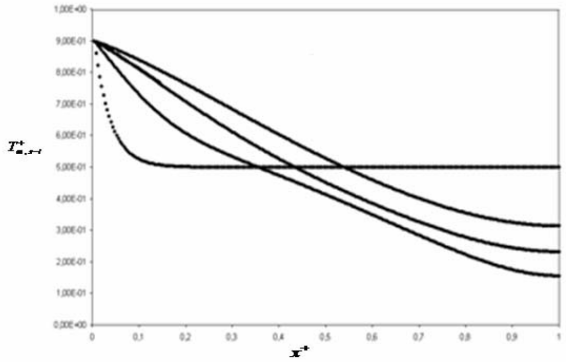

Figure 3. Dimensionless temperature distribution for the matrix during the hot period (summer). The set of data lines shows progression to the steady state from initial point.

Figure 4 presents the variation of the sensible effectiveness with the number of cycle of the wheel for the summer run. It is clear from this figure that the effectiveness value changes in exponential fashion until it reaches the cyclic equilibrium. The wheel reaches the steady state after about 50 cycles. It is to be noted here that the same profile of the sensible effectiveness was obtained for the winter run. A fast rotating sensible wheel requires more rotations before reaching the steady state operation because the time for each cycle becomes small.

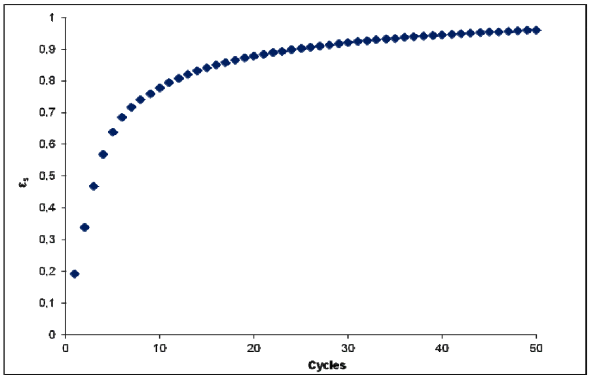

Figure 4. Variation of the sensible effectiveness with the number of cycle (summer).

Figure 5 illustrates the effect of the flow rate volume on the wheel effectiveness at different matrix porosity. It can be observed that at a low value of flow rate volume 150 [CMH], the wheel effectiveness decreases from 0.94 to 0.90 with increasing matrix porosity from $\varphi = 90\%$ to 93%, respectively. However, at a high value of flow rate volume 300 [CMH], the effectiveness decreases from 0.91 to 0.86 with increasing matrix porosity from $\varphi = 90\%$ to 93%, respectively. The sensitivity of the wheel effectiveness to the matrix porosity increases in terms of the volume flow rate.

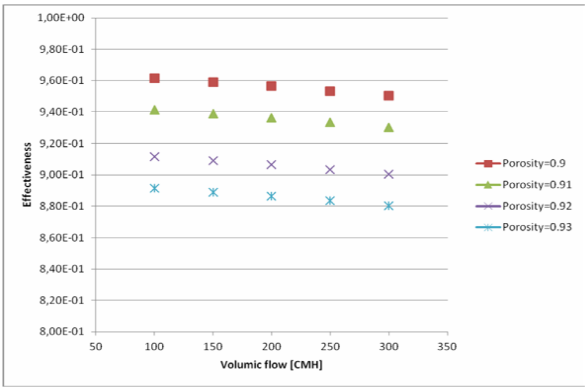

Figure 5. Variation of sensible effectiveness with volume flow rate for different porosity.

To use the rotational speed of the wheel as a control method, the extensive study of the influence of Ω on wheel performance should be therefore enhanced. Numerical investigation of the effect of the rotational speed of the wheel effectiveness is hereafter investigated. The effectiveness correlation using limiting case $(\Omega \to 0, \infty)$, and $\varepsilon - NTU$ methods are compared.

Table 3 shows a satisfactory agreement between the present numerical results and those reported elsewhere [9]:

Table 3. Comparison of both our results and those of Kabeel [9]

Volumic flow [CMH]	Effectiveness for present results	Effectiveness for previous work [9]
100	0.96	0.92
150	0.958	0.89
200	0.95	0.85
250	0.94	0.82

Figure 6 shows the effect of the rotational speed Ω on the effectiveness with a specified value of NTU_{HT}. It is concluded from the numerical results that the effectiveness increases with increasing C_r^+ in this figure up to a certain limit. Such limit is selected according to other previous works.

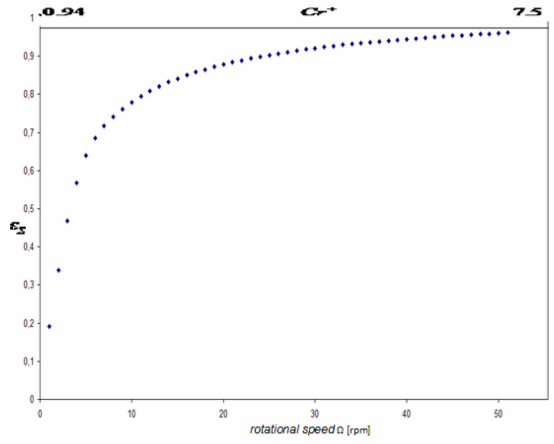

Figure 6. Variation of sensible effectiveness at low rotational speed Ω.

The number of transfer units (NTU) is defined as the ratio of convective heat transfer to the air temperature potential:

$$NTU_{HT} = \frac{h_{HT} A_s}{(\dot{m} Cp_g)}.$$

The effect of NTU on the sensible effectiveness is shown in Figure 7. As it can be seen, ε_s is an increasing function of NTU. This is due to the increase in NTU with decreasing mass flow rate.

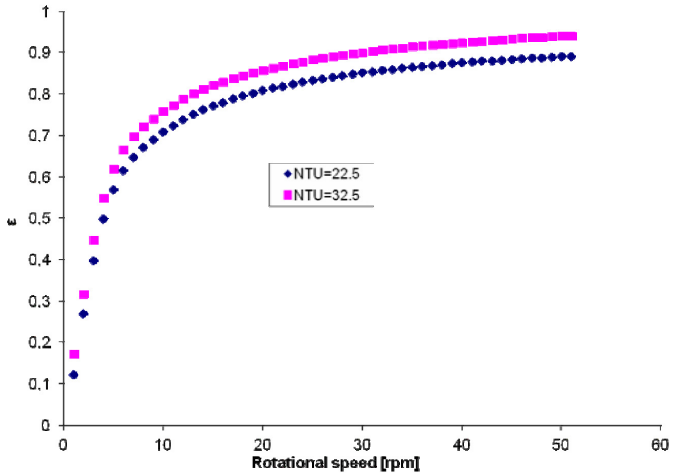

Figure 7. The variation of sensible effectiveness with rotational speed for two different NTU values.

For the condensation model, we note that the temperature profiles of solid matrix and gas are similar to those of the sensible model. However, the effectiveness is seriously influenced by the operating conditions. The variation of the wheel effectiveness (sensible, latent and total) as a function of the wheel cycle is presented in Figure 8.

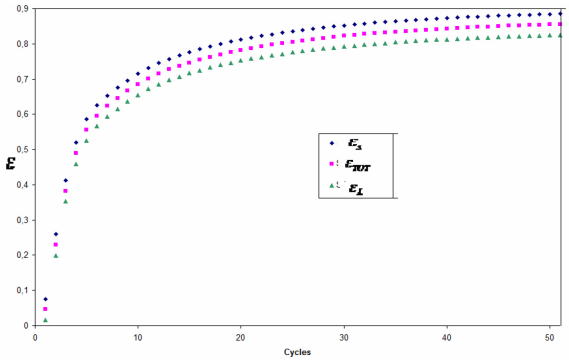

Figure 8. Wheel effectiveness (sensible, latent and total) as a function of wheel cycle.

As it can be seen, ε_s, ε_L and ε_T all increase with the increasing wheel cycle but they increase more rapidly when the cycle number is in the range of 0-50. The sensible effectiveness is larger than the latent effectiveness regardless of the wheel cycle. This indicates that the moisture transfer uses some of the thermal energy. It is to be noted here that during summer and winter operations, the sensible model leads to the same behavior of the effectiveness.

5. Conclusion

A numerical model was developed to simulate heat and mass transfer for condensation model. The influence of some operating parameters on the effectiveness of the wheel was analyzed. The temperature profiles of gas and solid matrix have shown that there is a transfer of heat and moisture from one air stream to another. The effectiveness values change in exponential fashion until they reach the cyclic equilibrium after approximately 50 cycles. Also, the sensible effectiveness values from the condensation model are lower than those of the sensible model. This indicates that the moisture transfer processes consume some of the thermal energy which is not available in sensible transfer. Further studies are in progress to reach the effect of the pressure and lost on energy inside such wheel. These parameters have indeed played an important role in heat and mass transfer in this condensation wheel.

References

[1] J. G. Van Leersum and C. W. Ambrose, Comparisons between experiments and a theoretical model of heat and mass transfer in rotary regenerators with nonsorbing matrices, J. Heat Transfer 103 (1981), 189-195.

[2] C. J. Simonson, D. L. Ciepliski and R. W. Besant, Determining the performance of energy wheels: Part I experimental and numerical methods, ASHRAE Trans. 105 (1999), 174-187.

[3] Ephrahim M. Sparrow, Heat and mass transfer characteristics of a rotary regenerative total energy wheel, International Journal of Heat and Mass Transfer 50 (2007), 1631-1636.

[4] M. Ali Mandegari and H. Pahlavanzadeh, Introduction of a new definition for effectiveness of desiccant wheels, Energy 34(6) (2009), 797-803.

[5] I. L. Maclaine Cross, A theory of combined heat and mass transfer in regenerators, Ph.D. Dissertation in Mechanical Engineering, Monash University, Australia, 1974.

[6] J. G. Van Leersum, Heat and mass transfer in regenerators, Ph.D. Dissertation in Mechanical Engineering, Monash University, Australia, 1975.

[7] C. J. Simonson and R. W. Besant, Energy wheel effectiveness: part I-development of dimensionless groups, International Journal of Heat and Mass Transfer 42(12) (1999), 2161-2170.

[8] M. H. Ahmed and N. M. Kattab, Evaluation and optimization of solar desiccant wheel performance, Renewable Energy 30 (2005), 305-325.

[9] A. E. Kabeel, Solar powered air conditioning system using rotary honeycomb desiccant wheel, Renewable Energy 32 (2007), 1842-1857.

[10] Abdulmajeed S. Al-Ghamdi, Analysis of air-to-air rotary energy wheels, Thèse de doctorat, Ohio University, June 2006.

[11] C. E. L. Nobrega and N. C. L. Brum, Modeling and simulation of heat and enthalpy recovery wheels, Energy 34(12) (2009), 2063-2068.

[12] American Society of Heating, Refrigeration and Air Conditioning Engineers ASHRAE, Handbook of Fundamentals, New York, 2001.